Nonlinear Analysis of Heterogeneous Model for an Industrial Ammonia Reactor

Article *in* Chemical Product and Process Modeling · January 2009

DOI: 10.2202/1934-2659.1296 · Source: OAI

4 authors, including:

Erasmo Mancusi
Università degli Studi del Sannio
64 PUBLICATIONS **292** CITATIONS
SEE PROFILE

Pier Luca Maffettone
University of Naples Federico II
153 PUBLICATIONS **2,629** CITATIONS
SEE PROFILE

Chemical Product and Process Modeling

Volume 4, *Issue* 2 2009 *Article* 5

MODELING AND CONTROL

Nonlinear Analysis of Heterogeneous Model for an Industrial Ammonia Reactor

Erasmo Mancusi* Pier Luca Maffettone†

Francesco Gioia‡ Silvestro Crescitelli**

*Università del Sannio, mancusi@unisannio.it

†Università degli Studi di Napoli Federico II, pierluca.maffettone@unina.it

‡Università degli Studi di Napoli Federico II, francesco.gioia@unina.it

**Università degli Studi di Napoli Federico II, silvestro.crescitelli@unina.it

Nonlinear Analysis of Heterogeneous Model for an Industrial Ammonia Reactor

Erasmo Mancusi, Pier Luca Maffettone, Francesco Gioia, and Silvestro Crescitelli

Abstract

Ammonia production is generally carried out in multiphase catalytic reactors. In this paper we analyze an industrial reactor for ammonia production with a dynamic heterogeneous model that accounts for transport resistance both inside and outside catalyst pellets. The work is aimed at investigating the possible appearance of periodic solutions in normal operating conditions for their relevance in terms of safety and control strategy. The analysis is based on a continuation approach to determine the bifurcational characterization of model predictions. This description is compared with that derived in a previous work (Mancusi et al. 2000), which was based on a simpler pseudo-homogeneous model of the same process.

KEYWORDS: bifurcation theory, nonlinear analysis, ammonia reactor, control

Introduction

It is well known that a complete dynamical characterization of an industrial process is needed to detect complex nonlinear phenomena, such as multiplicity and periodic solutions, which can affect process design and operation (Seider et al., 1999). Such an analysis can give valuable information to develop adequate control strategies (Recke et al., 2000).

Multiplicity and periodic behaviors in normal operating conditions of ammonia reactors have been repeatedly mentioned in the literature (Naess et al., 1993; Morud, 1995; Morud and Skogestad, 1998; Andersen, 2000). Morud and Skogestad reported observations of oscillations in an industrial ammonia reactor. In that case, large amplitude temperature oscillations were observed as a result of a sudden decrease of the reactor pressure occurred during normal operations. As a consequence, the catalyst was damaged. Morud and Skogestad analyzed the process with a pseudo-homogeneous dynamic model, and proved that periodic solutions emerge from a Hopf bifurcation. The loss of stability of the high conversion stationary solution was predicted to occur at 170 bar in good qualitative agreement with accident data. Their analysis was performed by linearizing the model close to steady state solutions, and confirmed the limitations of Van Herden (1953) approach to process stability analysis (e.g., Aris and Amundson, 1958; El Nashaie and Elshishini, 1996). Later, Mancusi et al. (2000) presented a complete dynamical characterization of the same model. In that case, the nonlinear model was analyzed with a parameter continuation approach. The appearance of periodic regimes from a supercritical Hopf bifurcation was confirmed; moreover, the coexistence of stable periodic regimes and stationary solutions at high pressure (up to 160 bar) was shown, and the catastrophic nature of the Hopf bifurcation was also illustrated.

Pseudo-homogeneous models are certainly attracting for their simplicity, but they are obviously unable to account for any intraparticle and interphase phenomena. In heterogeneously catalyzed reactions, mass and heat transfer between gas and catalyst surface and the presence of gradients within catalyst are often relevant. In fact, whenever chemical active centers are dispersed throughout inner surface of a porous catalyst, reactant/product diffusion within the catalyst pores can play a role. In the case of ammonia converters, catalyst pellets are usually 6-10 mm in size. Therefore, intraparticle mass transfer resistance must be considered (Elnashaie and Elshishini, 1993).

In this work, we extend the non-linear analysis proposed in Mancusi et al. (2000) by modeling the ammonia reactor accounting for intraparticle and interparticle phenomena. A thorough description of the attractors both static and dynamic is made available for typical operating conditions. The inlet temperature and the reactor pressure are considered as bifurcation parameters. Finally we

perform a comparison between the predictions of the most general heterogeneous model presented in this work and the simplest pseudo-homogeneous model previously studied (Mancusi et al., 2000).

Mathematical model and numerical solution technique

The reactor consists of a series of three adiabatic beds. Cooling is supplied with cold fresh feed, and feed preheating with effluents. Figure 1 shows a schematic of the system. The heat exchanger and the mixers are assumed to have no dynamics, since the reactant residence time within both of them is small if compared with that in the catalytic fixed beds. The same assumptions were made by Morud and Skogestad. The kinetics for the reaction $N_2 + 3\,H_2 \Leftrightarrow 2\,NH_3$ are modeled as suggested by Froment and Bischoff (1990) (see Notation for all symbols):

$$\mathrm{r}_{N_2} = \frac{1}{\rho_s}\left(k_1 p_{N_2} \frac{p_{H_2}^{1.5}}{p_{NH_3}} - k_{-1} \frac{p_{NH_3}}{p_{H_2}^{1.5}} \right)$$

The heterogeneous model is derived by writing mass and energy balances in both gas and solid phases. An ordering analysis (see Appendix) shows that gas axial diffusion is negligible with respect to convective transport in each adiabatic bed ($Pe \approx 2000$), and, as a consequence, gas phase can be considered in plug flow. Inter-phase transport resistance is negligible for the large gas velocities ($Bi_d \approx 1000$). On the contrary, temperature gradient between solid and gas phase cannot be neglected. Within the catalyst pellets, mass and energy are transported by diffusion. The main constituent of the catalyst is iron, and its high thermal conductivity makes the temperature gradients inside the pellet negligible. This is confirmed by a Prater analysis, in fact for the system at hand the Prater number β is very small ($\beta < 10^{-3}$). Finally, since the Lewis (*Le*) number is very large, quasi-steady state assumption holds for mass balance within catalyst.

Within the above assumptions, the model consists in the following dimensionless equations:

MASS BALANCE FOR GAS PHASE AND INLET CONDITION ON ANY ADIABATIC BED

$$0 = -w\frac{\partial \omega_g}{\partial z} + \rho_s r_c\left(\omega_g; T_g\right)\eta; \qquad \omega_g\left(0,t\right) = \omega_{in} \qquad (1)$$

ENERGY BALANCE FOR CATALYST PARTICLES AND BOUNDARY CONDITIONS ON ANY ADIABATIC BED

DOI: 10.2202/1934-2659.1296

$$\varepsilon_g \rho_g c_{pg} \frac{\partial T_g}{\partial t} = -w c_{pg} \frac{\partial T_g}{\partial z} - h_f a_v \left(T_g - T_s\right); \qquad T_g\left(0,t\right) = T_{in} \tag{2}$$

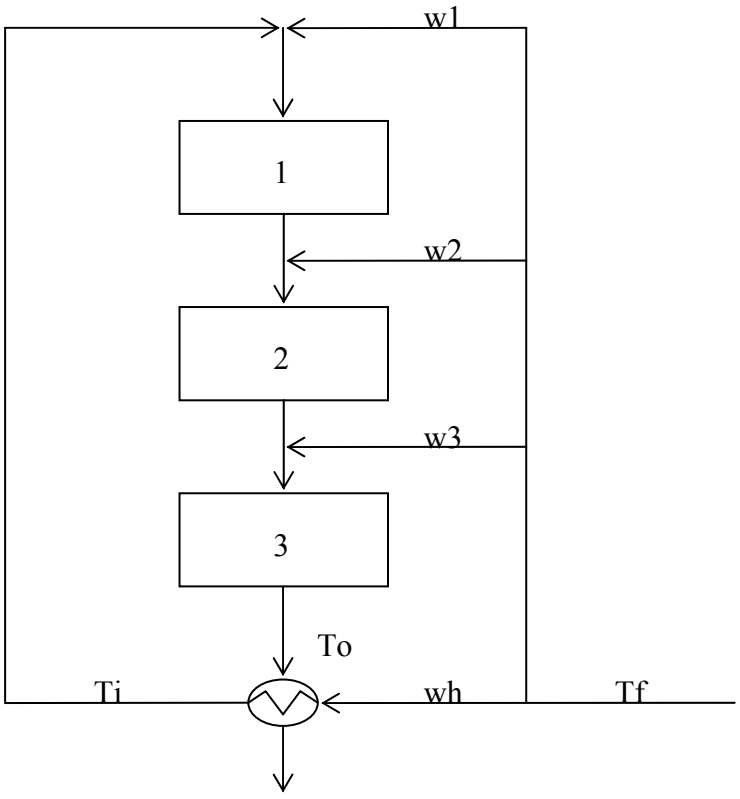

Figure 1 - The sketch of the ammonia reactor

MASS BALANCE FOR CATALYST PARTICLES AND BOUNDARY CONDITIONS

$$\begin{aligned} 0 &= \frac{D_{NH_3,eff}\rho_g}{r^2}\frac{\partial}{\partial r}\left(r^2 \frac{\partial \omega_s}{\partial r}\right) + \rho_s r_c\left(\omega_s; T_s\right); \\ \omega_s\big|_{r=R_p} &= \omega_g, \ \left.\frac{\partial \omega_s}{\partial r}\right|_{r=0} = 0 \end{aligned} \tag{3}$$

ENERGY BALANCE FOR CATALYST PARTICLES

$$\rho_s c_{ps} \frac{d T_s}{d t} = h_f a_v (T_g - T_s) + \rho_s \left(-\Delta H\right) \ r_c\left(\omega_g; T_g\right)\eta \tag{4}$$

In Eq. (1) the gas-phase hold-up is neglected. This assumption was supported by preliminary results obtained by accounting for gas hold-up that showed to be negligible. In Eq. (3), the effective diffusivity ($D_{NH_3,eff}$) is assumed to be constant at its bulk value. Since Eq. (3) is written in mass terms, it does not contain any effect due to volume changes. The effect of internal and external resistances on the reaction rate are accounted for by using an effectiveness factor η, which takes into account also the temperature difference between the two phases, defined as (Froment and Bischoff, 1990):

$$\eta = \frac{\text{actual rate of reaction}}{\text{rate of reaction at bulk conditions}} = \frac{3\int_0^{R_p} r^2\, r_c\left(\omega_s;T_s\right)dr}{R^3{}_p r_c\left(\omega_g;T_g\right)} \tag{5}$$

Usually, a pseudo-homogeneous model can be correctly implemented when η is close to one. This is not the case for ammonia converters. In Figure 2 (a) typical effectiveness factor profiles along the three beds at the industrial operating conditions are reported. It is worth noting that the effectiveness factor is always substantially smaller than unity. This fact demonstrates that a realistic modeling of ammonia converters must include intra particle diffusion and thermal inter phase resistances.

The efficiency factor is a function of the diffusional resistances, the reaction rate under the bulk conditions and the equilibrium constant (Elnashaie, 1989). The non monotonic η profile along the three fixed-bed catalytic reactors (Fig. 2(a)) can be explained by the interaction between the change along the axial coordinate of the intrinsic rate of reaction, the effective diffusivity and the equilibrium constant. The intrinsic rate of reaction ant the effective diffusivity increase with temperature, while the constant equilibrium decreases. The increase on the intrinsic rate of reaction obviously reduces the effectiveness factor while the increase of the effective diffusivity increases the effectiveness factor. Finally, as demostrated by Elnashaie et al. (1989), the effectiveness factor increases as the equilibrium constant increases. As Shown in Fig. 2(c) the intrinsic the diffusivity increases in the first reactor, while the intrinsic reaction rate firstly decrease and the increase (Fig. 2(b)). These two effect according with the decrease of the equilibrium constant (Fig. 2(d)) can explain the non-monotonic behavior of the effectiveness factor. In the second reactor the sharp increase of the intrinsic reaction rate (Fig.2(b)) together with the decrease of the equilibrium constant (Fig. 2(d)) overcame the effect of increase of the effective diffusivity (Fig. 2(c)) thus determining a reduction of the effectiveness factor (Fig. 2(a)). In the third

DOI: 10.2202/1934-2659.1296

reactor the effective diffusivity stays constant (Fig. 2(c)) while the intrinsic reaction rate decreases (Fig. 2(b)) but the sharp decrease of the equilibrium constant (Fig. 2(d)) apparently dominate this effect and the effectiveness factor is observed to slight decrease in the very first part of the third catalytic bed (Fig. 2(a)).

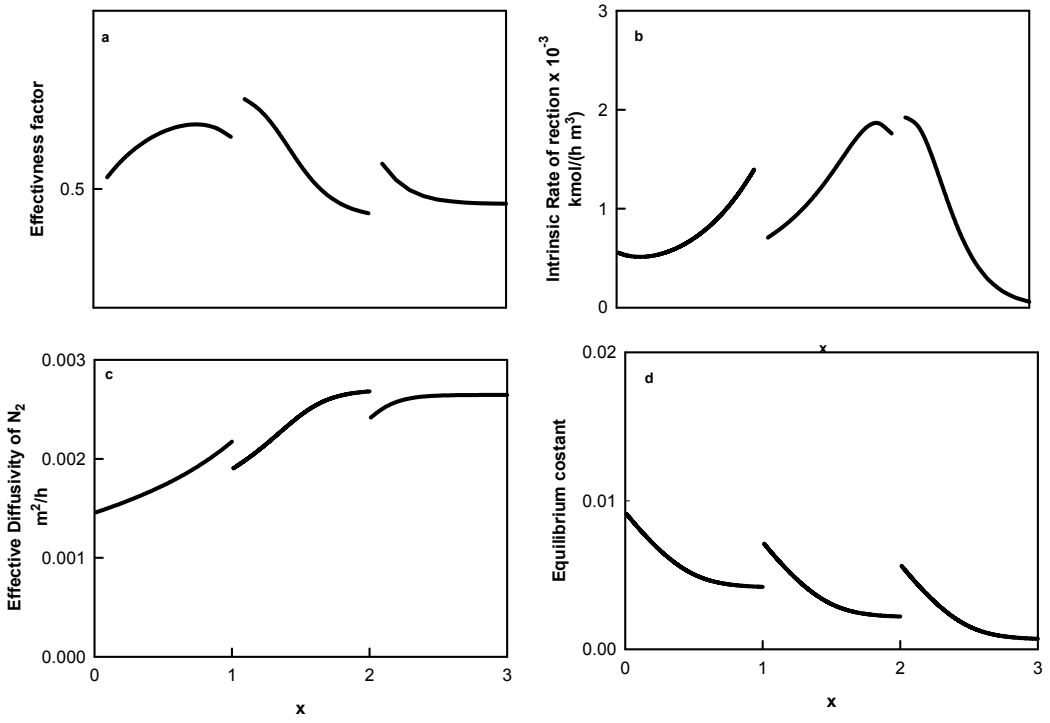

Figure 2 – (a) Effectiveness factor profile; (b) intrinsic reaction rate; (c) Effective diffusivity (d) equilibrium constant. (P=200 bar, T_f=240 C).

The numerical analysis of Eqs. (1)-(5) has been performed reducing the system of partial differential integral equations (PDIE) to a set of differential and algebraic equations (DAE). The domain of the spatial variable z in Eqs. (1)-(2) has been discretised on a grid of equally spaced points; 30 points are sufficient to ensure a grid-independent solution. The pellet mass balance Eq. (3) has been treated with orthogonal collocation methods (Villadsen and Michaelsen, 1978). It turned out that 3 collocation points were sufficient to ensure convergence, since the concentration profiles are always smooth. Eq. (4) it is just an ordinary differential equation. The integral (Eq. (5)), is calculated with an accurate Radau-Labotto quadrature (Villadsen and Michaelsen, 1978). As a consequence, the partial differential integral equations system (PDIE) (1)-(5) is transformed into a

differential algebraic equations (DAE) problem: the algebraic system of non-linear equations has been solved through an homemade routine based on Newton scheme while the integration in time of the differential part of the system has been performed implementing the Fortran routinesVODE (Brown et al., 1989). Both relative and absolute tolerances are set to the square root of the working machine precision.

The reduced mathematical model is studied with two different approaches: A continuation analysis is performed with the popular code AUTO97 (Doedel *et al.* 1997), and simulations are used to elucidate transient behaviors. The user defined routines for the continuation software were developed with *Mathematica*™ (Mancusi et al., 2000). With this technique, cumbersome algebra required to generate the right-hand sides of the dynamic model was easily performed. The subroutines for effectiveness factor computation were also linked to AUTO97 code.

Results

The bifurcation study was carried out by considering as bifurcation parameters the feed temperature T_f, and the reactor pressure P. These are important operating parameters as variation of such parameters may induce reactor ignition or shut off, and can be used as manipulated variable in a control law. Thus, the knowledge of the bifurcation behavior of the reactor is important as it allows a quick and complete characterization of reactor performances in terms of ignition switch off and coexistence of different regime solutions.

The continuation results are presented with two kinds of plots: solution diagrams for the bifurcation parameter T_f, and the bifurcation diagram in the plane T_f-P. The solution diagrams report versus the feed temperature the temperature of the gas coming out from the reactor. In the case of limit cycles, the maximum outlet-temperature value attained during the oscillations appears in the plots. On the other hand, the bifurcation diagram illustrates the loci of bifurcation points in the parameter space (Kubiçek and Marek, 1983). Some simulation results are also reported to illustrate interesting situations. Parameter values are typical of operating conditions and are reported in Table I.

Gas heat capacity, C_{pg}	3500 J kg^{-1} C^{-1}
Heat capacity of catalyst, C_{ps}	1100 J kg^{-1} C^{-1}
Heat of reaction, $-\Delta H$	$2.7*10^{6}$ J kg^{-1}
Dispersion coefficient, bed 1 Γ_1	$5.6*10^{-4}$ m^2 s^{-1}
Dispersion coefficient, bed 2 Γ_2	$4.6*10^{-4}$ m^2 s^{-1}
Dispersion coefficient, bed 3 Γ_3	$3.3*10^{-4}$ m^2 s^{-1}
Mass flow through heat exchanger, W_h	127 tons hr^{-1}

DOI: 10.2202/1934-2659.1296

Quench bed 1, W_1	58 tons hr^{-1}
Quench bed 2, W_2	35 tons hr^{-1}
Quench bed 3, W_3	32 tons hr^{-1}
Inlet mole fraction NH_3 (stechiometric feed)	0.04
Typical reactor pressure, P	200 bar
Typical inlet gas feed temperature, T_f	240 C
Volume, bed 1	6.69 m^3
Volume, bed 2	9.63 m^3
Volume, bed 3	15.2 m^3
Bed void fraction, ε_g	0.4475
Catalyst/gas heat transfer coefficient, bed 1 $h_f a_v$	5.3 * 10^5 W $m^{-3}K^{-1}$
Catalyst/gas heat transfer coefficient, bed 2 $h_f a_v$	4.4 * 10^5 W $m^{-3}K^{-1}$
Catalyst/gas heat transfer coefficient, bed 3 $h_f a_v$	3.3 * 10^5 W $m^{-3}K^{-1}$
Catalyst bulk density, ρ_s	2200 kg m^{-3}
Typical gas density, ρ_g	50 k kg m^{-3}
Porosity, ε_s	0.52
Tortuosity, τ	7.
Catalyst radius, R_p	0.003 m
Thermal conductivity, λ_{eff}	0.65 KJ kg^{-1} C^{-1}

TABLE I - Parameters used in this work (Morud, 1995; Dyson and Simon, 1968; Elnashaie and Elshishini, 1993)

The solution diagram, shown in Fig. 3, reports for P=200 bar the outlet gas temperature versus the bifurcation parameter, T_f. Bifurcation conditions are reported in Table II.

	T_f (C)
S1	209.45
S2	329.55
H1	211.76
H2	253.60
F1	210.98
F2	241.85
F3	207.35

Table II- Values of the inlet temperature T_f at the bifurcations points shown in Fig. 3

A stable periodic solution branch is close to normal operating conditions (see the inset in Fig. 3). This branch, emerging from the supercritical Hopf bifurcation (H1), is initially stable; then, after a fold bifurcation (F1), the periodic solution becomes unstable; a second fold bifurcation (F2) makes the solution stable again. The presence of two folds (F1 and F2) has an important effect, which was already reported in Mancusi et al. (2000). Indeed, although the Hopf bifurcation (H1) is supercritical than theoretically non-catastrophic, the presence of F1 and F2 makes the situation "catastrophic" since any small feed temperature reduction larger than $|\Delta T_f| = |T_{f\,H1} - T_{f\,F1}|$ results in the jump from a stable static solution to the stable periodic solution with large amplitude oscillations (the stable branch between F2 and a third fold F3). In fact, close to H1, a small change in feed temperature leads to large excursion in the bed temperature. This scenario is reported in Figure 4.

Initially, the reactor operates at steady state with T_f=212C at t=100 min the feed temperature is reduced of 0.5C. The system becomes unstable and exhibits limit-cycle behavior. A decrease in the feed temperature from 212C to 211.5C leads to a periodic regime, but, though very close to a supercritical (hence, non-catastrophic) Hopf bifurcation H1, the emerging oscillations are of large amplitude. In fact, these periodic regimes are those emerging from catastrophic Fold F1 and not from supercritical Hopf H1.

DOI: 10.2202/1934-2659.1296

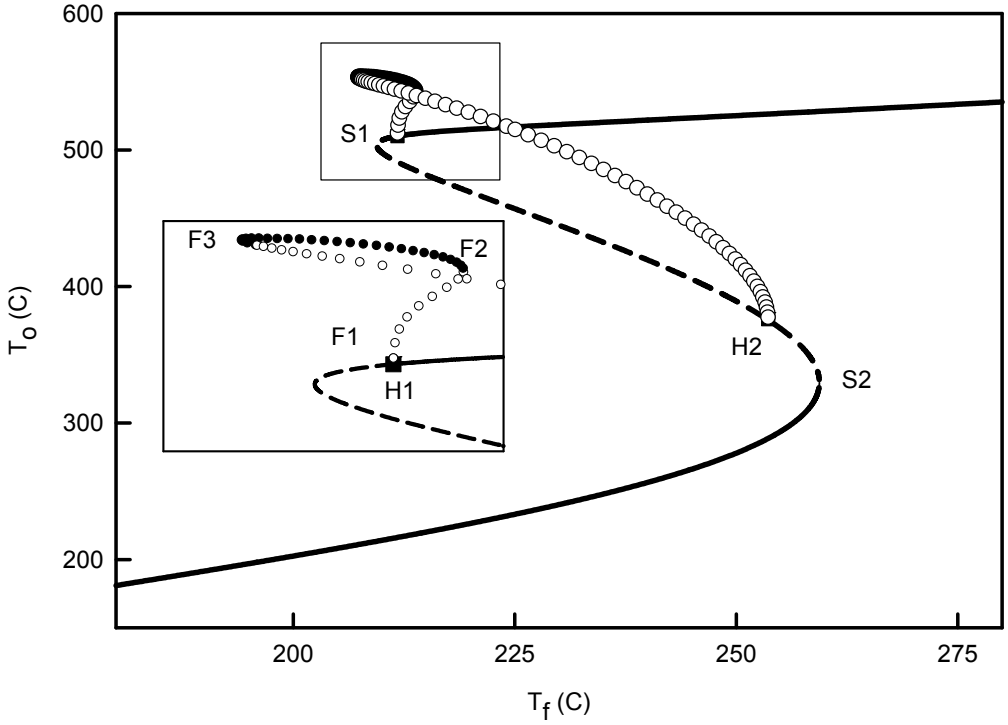

Figure 3 - The solution diagram for the heterogeneous model. Solid lines stable stationary solutions; dashed lines unstable stationary solutions; filled circles stable limit cycles; unfilled circles unstable limit cycles; filled squares Hopf bifurcations. The inset shows details of the delimited rectangular region.

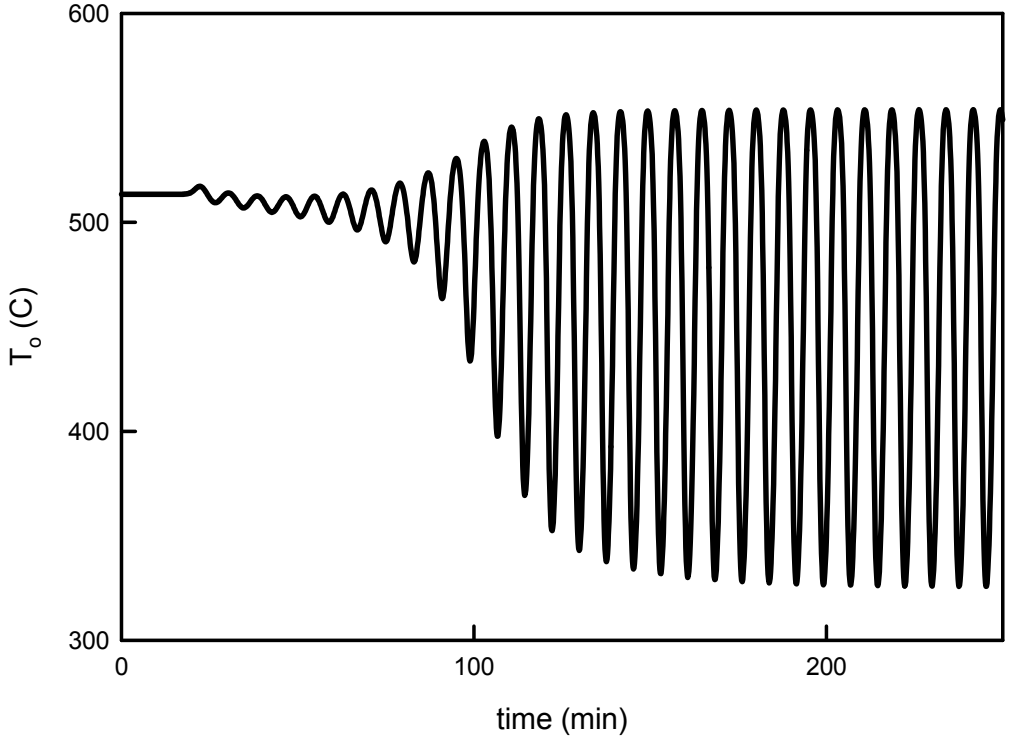

Figure 4 – The transient of out coming temperature (To C) following a step decrease (0.5 C) of feed temperature at time 100min.

The effect of stable periodic regimes can be explained by the spatio-temporal pattern reported in Figure 5. In Fig. 5, the horizontal coordinate is the dimensionless axial position, and the vertical coordinate is the time. The level of temperature is color coded. As consequence of stable periodic regime pulsing travelling waves across the three adiabatic fixed beds appear. The temperature front forms in the first reactor, and then moves along axially. The amplitude of temperature oscillations is wide and this could cause thermal stress of the catalyst.

DOI: 10.2202/1934-2659.1296

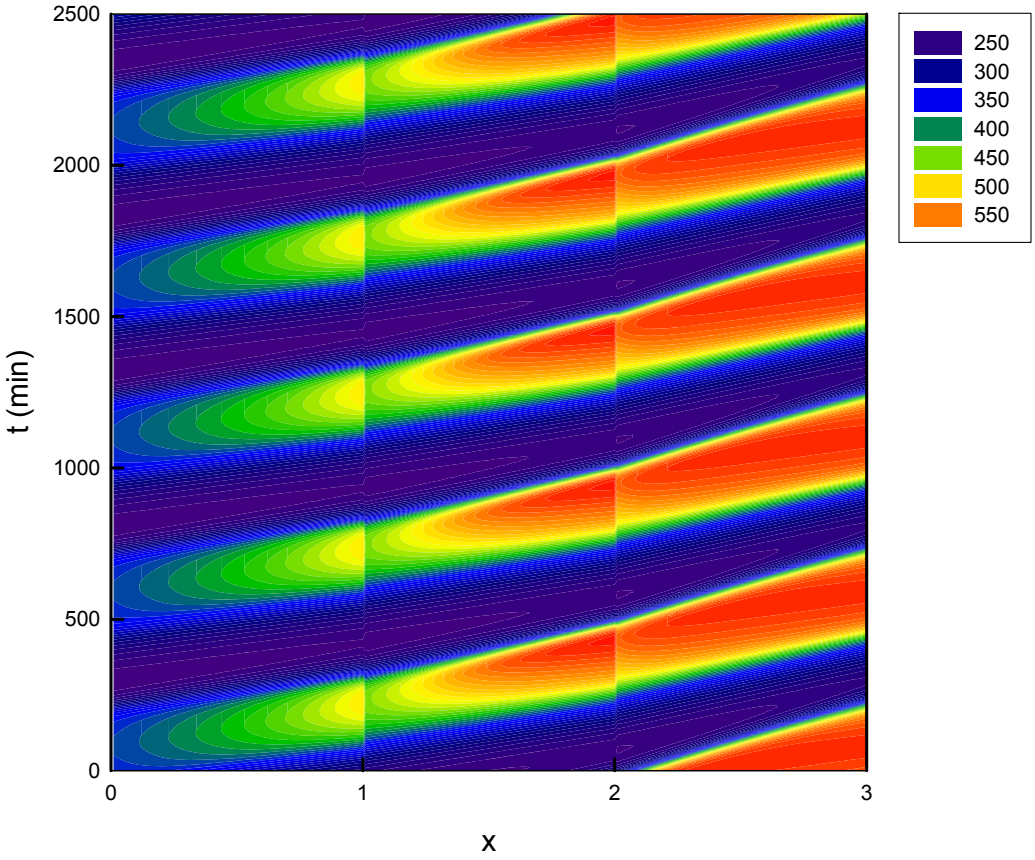

Figure 5 – Spatio-temporal patterns of the solid phase temperature for T_{in}=210 C and P=200 bar.

Finally, at $T_f = T_{f\,F3}$ a fold (F3) marks the onset of an unstable branch that eventually dies out onto another supercritical Hopf bifurcation (H2). The fold bifurcation F3 plays an important role, as well. In fact, a decrease in the feed temperature from its set point is "recoverable" if T_f does not go below the leftmost fold bifurcation value ($T_{f\,F3}$). If, on the other hand, the fold is surpassed ($T_f < T_{fF3}$), then the model predicts the jump to the low conversion branch. A subsequent increase of the feed temperature would result in a new "start-up" route along the low conversion branch up to the limit point at $T_f = T_{f\,S2}$.

The effect of the reactor pressure P is addressed by a bifurcation diagram (Fig.6) where the loci of all the bifurcations described in Fig.3 are reported in the plane T_f-P .

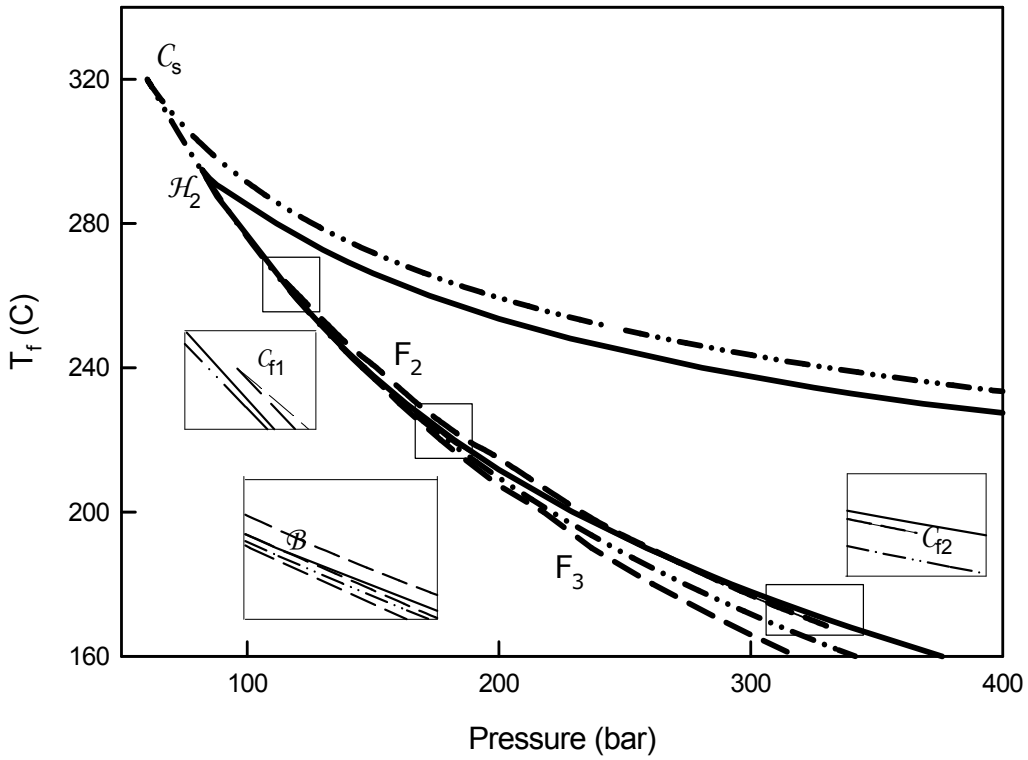

Figure 6 - The bifurcation diagram in the plane T_f-P for the heterogeneous model. The dashed-dotted lines represent the static saddle-node bifurcation; the solid lines represent the Hopf bifurcation conditions; the dashed lines represent the saddle-node bifurcation on the limit circles.

In this plot, the lines divide the parameter space in regions characterized by qualitatively similar phase portraits (Kuznetsov, 1997): solid lines represent Hopf bifurcations; double-dot-dashed lines represent limit point bifurcations, and dashed represents fold bifurcation (saddle-node on limit cycles) lines. The solution diagrams presented in Fig. 3 correspond to a horizontal cross section at a reactor pressure of 200 bar.

In Figure 6, the limit-point curves set the limits of a region with multiple steady states, while the Hopf curves encircle a region with a multiplicity of periodic solutions. Notice, however, that periodic solutions exist outside the Hopf regions as well, for the existence of cyclic fold bifurcations. When present, the bifurcation line related to F_2 marks the upper limit for existence of periodic solutions, whereas the line for F_3 represents the lower limit. The latter curve is important since it marks the shut-off conditions.

DOI: 10.2202/1934-2659.1296

Several codimension 2 bifurcations are encountered: the cusps C_s, C_{f1}, C_{f2}, Hopf-Hopf bifurcation ($\mathcal{H}_2$-bifurcation (Kuznetsov, 1997)), and the Bautin bifurcation ($\mathcal{B}$) (Kuznetsov, 1997).

Pseudo-Homogeneous Model

Figure 7 shows the solution diagram for the pseudo-homogeneous model at the very same conditions of Fig. 3. Bifurcation conditions are reported in Table III.

	T_f (C)
S1	205.16
S2	262.72
H1	214.14
H2	266.92
H3	210.43
H4	219.08
F1	213.87
F2	214.70
F3	187.24

Table III- Values of the inlet temperature T_f at the bifurcations points shown in Fig. 7

A qualitative similarity is evident between Fig. 3 and Fig. 7. Once again, a hysteresis is found both on the steady state branch and on the periodic branch. Again, the vicinity of H1 to F1 makes the Hopf bifurcation (H1) catastrophic, and the fold bifurcations F2 e F3 mark the "real" conditions of appearance/disappearance of stable periodic solutions. The only qualitative difference is the presence in Fig. 7 of two Hopf bifurcations (H3 and H4). These points are connected by a branch of unstable limit cycles. These solutions are saddle cycles, which play a significant role in the determination of basin of attractions of stable solutions. From a quantitative point of view, there are significant differences, however. The pseudo-homogeneous model predicts stable dynamic regimes down to 187C, a value significantly different from that predicted by the heterogeneous model (207C).

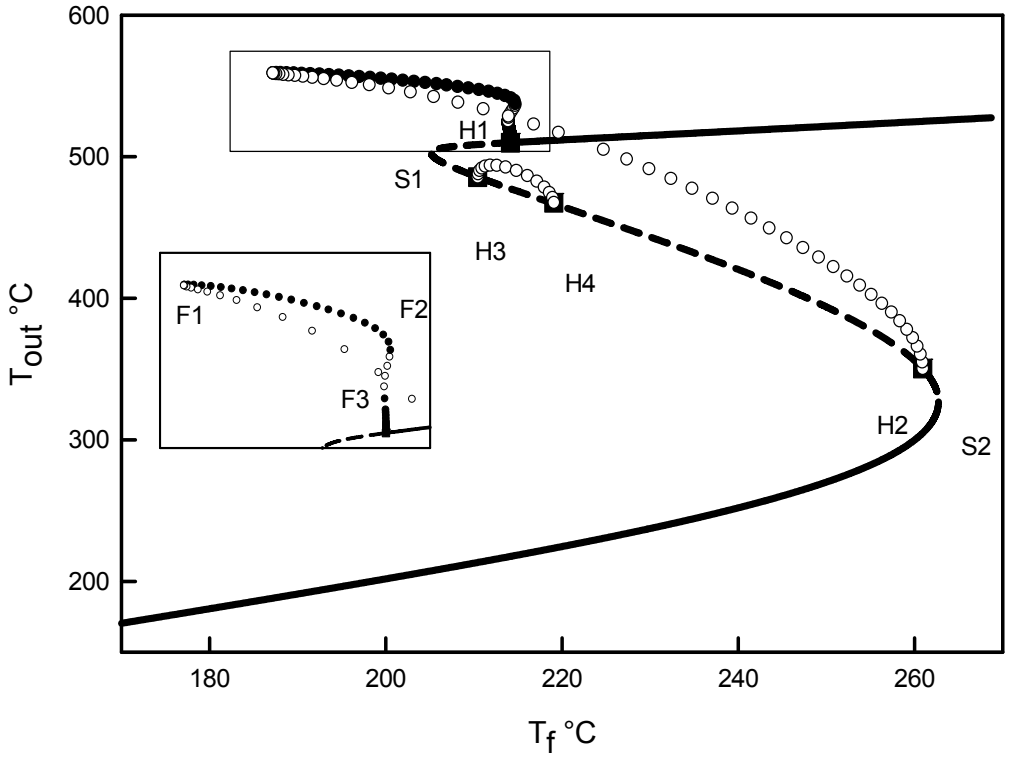

Figure 7- The solution diagram for the pseudo-homogeneous model for *P*=200 bar. Solid lines stable stationary solutions; dashed lines unstable stationary solutions; filled circles stable limit cycles; unfilled circles unstable limit cycles; filled squares Hopf bifurcations. The inset shows details of the delimited rectangular region.

Figure 8 shows the bifurcation diagram for the pseudo-homogeneous model. There is a qualitative similarity with the results obtained with the heterogeneous model, and even codimension 2 bifurcations are preserved. The main difference is the presence of a Hopf bifurcation line relative to Hopf bifurcation as H3 and H4 of Fig. 8.

DOI: 10.2202/1934-2659.1296

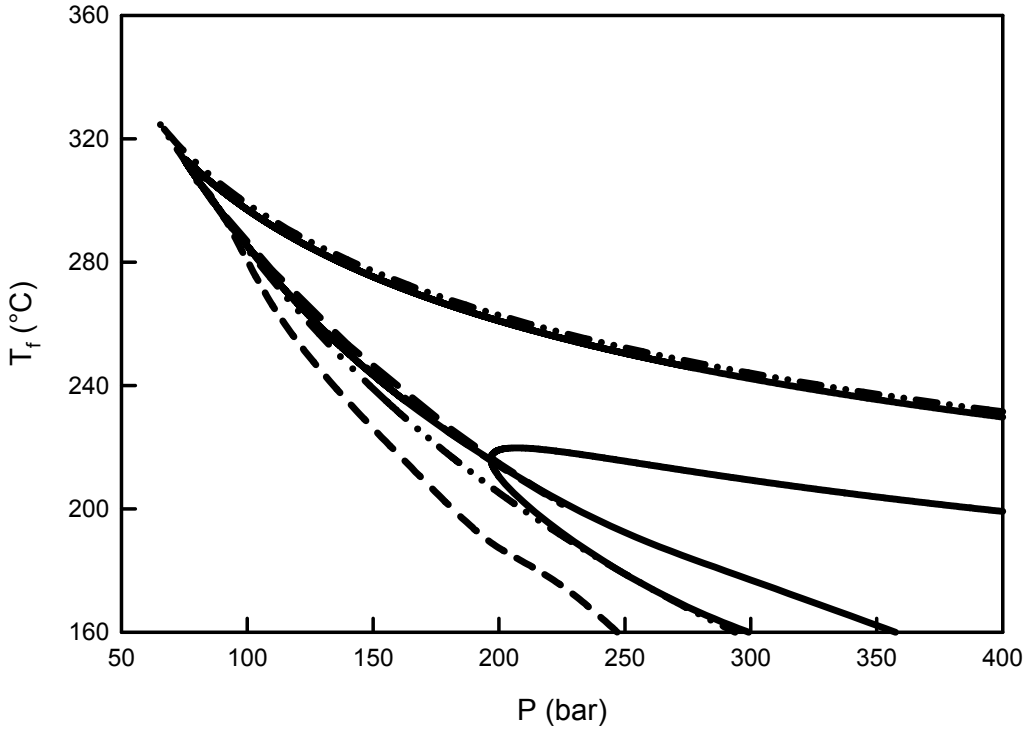

Figure 8 - The bifurcation diagram in the plane P-T_f for the pseudo-homogeneous model. The dashed-dotted lines represent the static saddle-node bifurcation; the solid lines represent the Hopf bifurcation conditions; the dashed lines represent the saddle-node bifurcation on the limit circles.

Conclusions

A heterogeneous model for an industrial ammonia plant has been studied with typical nonlinear tools. The model consists of two partial differential equations coupled with ordinary differential and algebraic equations. An *ad hoc* composite algorithm has been constructed to simulate the model, and the same discretization has also been used to perform a parameter continuation analysis.

Application of typical tools of nonlinear dynamic analysis allowed one to analyze complex situations as multiplicity and hysteresis on periodic branches. The identified fold bifurcations on the periodic branches represent the conditions of appearance/disappearance of stable limit cycles. This situation is predicted by considering as a bifurcation parameter both the reactor pressure and the feed temperature.

A comparison between pseudo-homogeneous and heterogeneous modeling has shown that from a qualitative point of view the predictions are similar. In both

cases, the loss of stability of high conversion static solutions is accompanied by the birth of stable limit cycles. The qualitative similarity between the two models can be explained by the fact that the relevant characteristic times are the thermal time and the residence time. The heterogeneous model introduces a new characteristic time related to the energy exchange between the two phases. This time scale is indeed short in typical operating conditions, and thus it does not alter the qualitative picture predicted by the pseudo-homogeneous modeling.

Finally, it is worth remarking that the predictions of the pseudo-homogeneous model are quantitatively different from those obtained with the heterogeneous model. An important difference is the reactor shut-down condition. For example, the shut-down feed temperature predicted with the heterogeneous model is ca. 207C, while with the pseudo-homogeneous model it is ca. 187C. This discrepancy could be obviously relevant in process control.

Appendix: Parameter estimation

A.1 Diffusivities

For the effective diffusivities in the catalyst pores, the parallel pore model of the catalyst structure is assumed (Satterfield, 1970; Aris, 1975):

$$\frac{1}{D_{i,eff}} = \frac{\tau}{\varepsilon_s}\left(\frac{1}{D_{i,m}} + \frac{1}{D_{i,K}}\right) \qquad \text{(A.1)}$$

Where D_{im} are the gas mixture diffusivities which account the unequal flux of the reactants while D_{iK} is the Knudsen diffusivities. In equation A.1 it is considered that the effective diffusivities contains the effect of the catalyst tortuosity and void fraction.

Due to the pore size distribution it is possible to neglect the Knudsen diffusivities (Satterfield and Scherwood, 1963), while the gas mixture diffusivities were calculated from a weighted average of the binary diffusion resistances (D_{ij}) and it can be derived from the Stefan-Maxwell diffusion equation (Krishna, 1989; Elnashaie, 1989):

$$\frac{1}{D_{im}^0} = \frac{1}{\sum_{j=1,i\neq j}^{n} \frac{1}{D_{ji}^0}\left(y_j - y_i \frac{z_j}{z_i}\right)} \qquad i = 1-3 \qquad \text{(A.2)}$$

where z represent the ratio of the molar flux of the component i to the mixture molar flux (Krishna, 1989):

DOI: 10.2202/1934-2659.1296

$$z_i = \frac{N_i}{N_1 + N_2 + N_3} \tag{A.3}$$

For the three components in the gas mixture (N_2 (1), H_2 (2), NH_3 (3)) z is determined by the reaction stoichiometry to be:

$$z_1 = \frac{1}{2};\ z_2 = \frac{3}{2};\ z_3 = -1$$

The binary diffusivities in A.2 are (Dyson and Simon, 1968);

$$D_{31}^0 = D_{13}^0 = 0.161$$
$$D_{32}^0 = D_{23}^0 = 0.571$$
$$D_{12}^0 = D_{21}^0 = 0.629$$

The diffusion coefficient calculated from equation A.2 are then corrected to the temperature and pressure of the reactor by the following equation (Dyson and Simon, 1968):

$$D_{im} = D_{im}^0 \left(\frac{T}{273} \right)^{1.75} \frac{1}{P} \tag{A.4}$$

where P is in *atm* and T in *Kelvin*.

A.2 Viscosities

The viscosity of the gas mixture is calculated by Wike's equation (Reid et al., 1977):

$$\mu_m = \sum_{i=1}^{3} \frac{y_i \mu_i}{\sum_{j=1}^{3} y_j \phi_{ij}} \tag{A.5}$$

where:

$$\phi_{ij} = \frac{1}{\sqrt{8}}\left(1+\frac{M_i}{M_j}\right)^{-1/2}\left[1+\left(\frac{M_j}{M_i}\right)^{1/4}\left(\frac{\mu_i}{\mu_j}\right)^{1/2}\right]^2 \qquad \text{(A.6)}$$

The pure gas viscosities are taken by Vagaftik et al. (1996) and are estimated at the normal operating conditions.

A.2 Conductivities

The thermal conductivity of each species are taken Vagaftik et al. (1996) and are calculated at the normal operating conditions, while the thermal conductivity of the gas mixture is calculated using the Lindsay and Bromley equation (Reid et al., 1977):

$$\lambda_m = \sum_{i=1}^{3} \frac{y_i \lambda_i}{\sum_{j=1}^{3} y_j A_{ij}} \qquad \text{(A.7)}$$

where:

$$A_{ij} = \frac{1}{4}\left[1+\sqrt{\frac{\mu_i}{\mu_j}\left(\frac{M_j}{M_i}\right)^{3/4}\frac{T+S_i}{T+S_j}}\right]^2 \frac{T+S_{ij}}{T+S_j} \qquad \text{(A.8)}$$

The required Sutherland constants (S_i and S_{ij}) are (Reid et al., 1977):

$S_1 = 116.025\ C$ $\qquad$ $S_{12} = 59.41\ C$

$S_2 = 30.42\ \ C$ $\qquad$ $S_{13} = 149.34\ C$

$S_3 = 359.72\ C$ $\qquad$ $S_{23} = 76.36\ C$

A.4 Mass and heat transfer coefficient

The following correlation (Satterfield e Sherwood; 1963) is used for k_c values:

$$J_m = \frac{0.458}{\varepsilon}\mathrm{Re}^{-0.407} = \frac{k_c \rho_g}{w} Sc^{2/3} \qquad \text{(A.9)}$$

DOI: 10.2202/1934-2659.1296

The heat transfer coefficient is also correlated with respect to the Reynolds number by-means of a *j*-factor expression:

$$J_h = \frac{h_f}{c_{pg} w} \mathrm{Pr}^{2/3} \qquad \text{(A.10)}$$

Taking $J_m = J_h$, the h_f value is calculated from (A.10).

A.5 External Temperature Gradient

The maximum temperature difference between the bulk fluid and the catalyst surface is derived by the following formula (Froment and Bischoff, 1990):

$$\frac{T_s - T}{T} = \beta_g \, Ca \left(\frac{Bi_d}{Bi_h} \right) \qquad \text{(A.11)}$$

We have assumed a constant temperature inside the catalyst pellet and so $T_s = T_s\big|_{r=R_p}$.

β_g is evaluated at he bulk fluid conditions. Assuming an average temperature and concentration in each catalyst bed we can evaluate the right side hand of the equation A.11. It is so possible to compute the maximum temperature difference between the two phase.

Notation

a_v	specific surface area of catalyst pellet, m^{-1}
Bi_d	Biot number for mass transfer, $k_c R_p / D_{eff}$
Bi_h	Biot number for heat transfer, $h_f R_p / \lambda_{eff}$
c_{ps}	catalyst specific heat, J $kg^{-1}K^{-1}$
c_{pg}	gas specific heat, J $kg^{-1}K^{-1}$
D_{eff}	effective diffusivity, m^2s^{-1}
D_K	Knudsen diffusivity, m^2s^{-1}
D_{im}	effective molecular diffusivity of *i* in a multicomponent mixture, m^2s^{-1}
h_f	heat transfer coefficient per unit particle surface area, W m^{-2} K^{-1}
H	reactor length, *m*
J_h	j-factor for heat transfer
J_m	j-factor for mass transfer
k_c	mass transfer coefficient, ms^{-1}
Le	Lewis number, $D_{eff} \rho_s c_{ps} / \lambda_{eff} \varepsilon_s$

M	molecular mass, kg kmol^{-1}
N	molar flux, kmol m^{-2}s^{-1}
P	reactor pressure, bar
p_i	partial pressure, bar
Pe	Peclet number, uH/Γ
Pr	Prandtl number, $c_p\mu/\lambda$
r	radial position in spherical particle
Re	Reynolds number, $d_p w/\mu$
R_p	Radius of catalyst pellet, m
r_c	reaction rate kmol kg^{-1} s^{-1}
Sc	Schmidt number, $\mu/\rho D$
T	temperature, C
T_f	Feed temperature, C
t	time, s
w	gas mass flux in the porosity interstices, kg m^{-2}s^{-1}
y	mole fraction
z	reactor axial coordinate
ΔH	heat of reaction, J $kg^{-1}_{NH_3}$
Γ	axial dispersion coefficient, m^{2}s^{-1}
β	Prater number, $\dfrac{(-\Delta H) D_{eff} \rho_g \omega_s\big\|_{r=R_p}}{\lambda_{eff} T_s\big\|_{r=R_p}}$
β_g	$\dfrac{(-\Delta H) D_{eff} \rho_g \omega_g}{\lambda_{eff} T_g}$
ε_g	void fraction of the bed
ε_s	void fraction of the catalyst pellet
η	effectiveness factor
λ	thermal conductivity, W m^{-1}K^{-1}
λ_{eff}	effective thermal conductivity of the catalyst pellet, W m^{-1}K^{-1}
μ	viscosity, Pa s
ρ_g	gas density, kg m^{-3}
ρ_s	catalyst density, kg m^{-3}
τ	tortuosity factor for catalyst
ω	ammonia mass fraction, $kg_{NH_3} kg^{-1}_g$

DOI: 10.2202/1934-2659.1296

Subscripts

g gas phase
i ith component
in bed inlet conditions
m mixture
s solid phase/catalyst

References

Andersen B. R., *Nonlinear dynamics of catalytic ammonia reactors*, Ph. D. thesis, Department of Chemical Engineering, Technical University of Denmark and Haldor Topsøe, 1999.

Aris R. and N. R. Amundson, "An analysis of chemical reactor stability and control", *Chem. Eng. Sci.*, **7**, 121, 1958.

Aris R., *The mathematical theory of diffusion and reaction in permeable catalyst*, Oxford University, Oxford, 1975.

Brown P. N., G. D. Byrne, and A. C. Hindmarsh, "VODE: a variable coefficient ODE solver," *SIAM J. Sci. Stat. Comput.*, **10**, 1038 1989.

Doedel E. J., Champneys A. R., Fairgrieve T. F., Kuznetsov Y. A., Sanstede B., and Wang X., *"AUTO97: continuation and bifurcation software for ordinary differential equations"*, July 1997.

Dyson D. C. e J.M. Simon, "A kinetic expression with diffusion correction for ammonia synthesis on industrial catalyst",. *Ind. Eng. Chem. Fundam*., **7,** 605, 1968.

Elnashaie S. S. E. H., and S. S. Elshishini, *Modeling, simulation and optimization of Industrial fixed bed catalytic reactors*, Gordon and Breach, Amsterdam, 1993.

Elnashaie S. S. E. H., and S. S. Elshishini, *Dynamical modeling, bifurcation and chaotic behavior of gas-solid catalytic reactors*, Gordon and Breach, Amsterdam, 1996.

Elnashaie S. S. E. H., "Non-monotonic behavior of the effectiveness factor along a catalyst bed", *Chem. Eng. Sci*., **44**, 1581, 1989.

Froment G. F. and K. B. Bischoff, *Chemical reactor analysis and design,* 2nd ed., Wiley, New York, 1990.

Krishna R., "Comments on "Simulation and optimization of an industrial ammonia reactor", *Ind. Eng Chem. Res*, **28**, 1266, 1989.

Kubiçek M. and M. Marek, *Computational Methods in Bifurcation Theory and dissipative structure,* Springer Verlag, New York, 1983

Kuznetsov Y. A., *Elements of applied bifurcation theory*, 2nd ed., Springer Verlag, New York, 1998.

Mancusi E., Merola G., Crescitelli S. and Maffettone P.L., "Multistability and hysteresis in an industrial Ammonia reactor", *AIChE J.*, **46**, 824 2000.

Morud J. C, *studies on the dynamics and operation of integrated plants,* Ph. D. thesis, University of Trondheim, The Nowegian Institue of Technology, 1995

Morud J. C., and Skogestad S., "Analysis of instability in an industrial ammonia reactor", *AIChE J.*, **44**, 888 1998.

Naess L., Mjaavatten A. and J. O. Li, " Using dynamic process simulation from conception to normal operation of process plants", *Computers Chem. Engng.*, **17**, 585 1993

Recke B., B.R. Andersen e S.B. Jorgensen, "Bifurcation control of sample chemical reaction systems", *ADCHEM 2000*, Italy, June 2000.

Reid R. C., Sherwood T. K. and E J. Prausnitz, *The properties of gases and liquids,* 3ed McRraw-Hill, New York, 1977.

Satterfield C.N. and T.K. Scherwood, *The role of diffusion in catalysis*, Addison-Wesley, Massachusetts, 1963.

Satterfield C.N., *Mass transfer in heterogeneous catalysis*, MIT, Cambridge, Massachusetts, 1970.

DOI: 10.2202/1934-2659.1296

Seider W. D., T. D. Seader, D. R. Lewin, *Process design principles: synthesis, analysis and evaluation*, Wiley, New York, 1999

Vagaftik N.B., Vinogradov Y.K. e V.S. Yargin, *Handbook of physical properties of liquids an gases*, Begell House, New York, 1996.

Van Herden C., "Autothermic processes. Properties and reactor design", *Ind. Eng. Chem.* **45**, 1242, 1953.

Villadsen J. and M.L Michelsen., *Solution of differential equation models by polynomial approximation*, Prentice-Hall, Englewood Cliffs, 1978.